Light-up nanostructures with allosteric DNA mimics of GFP

Tianqing Zhang,[1,9, †,*] Xinmin Qian,[2,3,4,†] Jiayi Zhang,[5,6] Huangchen Cui,[5,6] Tanxi Bai,[5,6] Wen Wang,[7] Yuxin Wang,[5,6] Zhaoli Gao,[8,*] Da Han,[1,*] Wenwen Zeng,[2,3,4,*] and Bryan Wei[5,6,*]

[1] Hangzhou Institute of Medicine, Chinese Academy of Sciences, Hangzhou, 310022, China.
[2] Tsinghua–Peking Joint Center for Life Sciences, Beijing, 100084, China.
[3] School of Basic Medical Sciences and Institute for Immunology, Tsinghua University, Beijing, 100084, China.
[4] Beijing Key Laboratory of Immunological Research of Allergy, Beijing, 100084, China.
[5] School of Life Sciences, Tsinghua University, Beijing, 100084, China.
[6] Center for Synthetic and Systems Biology, Tsinghua University, Beijing, 100084, China.
[7] BGI Research, Beijing, 102601, China
[8] Department of Biomedical Engineering, Chinese University of Hong Kong, Hong Kong, 999077, China.
[9] Leading contact: ztq.edu@gmail.com (T.Z.).
† These authors contributed equally to this work.
*Correspondence: ztq.edu@gmail.com (T.Z.), bw@tsinghua.edu.cn (B.W.), wenwenzeng@tsinghua.edu.cn (W.Z.), dahan@sjtu.edu.cn (D.H.) and zlgao@cuhk.edu.hk (Z.G.).

Abstract

In this study, we present a systematic approach for the rational design of synthetic allosteric DNA aptamers. This methodology enables precise control over the allosteric ON-OFF transition in fluorescent DNA aptamers, allowing for the engineering of aptamers with highly tunable fluorescent properties. When combined with toehold-mediated strand displacement, we have developed a series of allosteric aptamers in which the target sequence functions as a specific allosteric modulator. Furthermore, these aptamers have been applied in synthetic DNA computing and in the construction of responsive nanostructures that light up upon activation.

Keywords

Fluorescent DNA aptamer, allosteric regulation, DNA nanotechnology, DNA computing,

1. Introduction

Throughout millions of years of evolution, allostery has become a highly efficient and adaptable mechanism for molecular stimulus response, regulating many essential life processes such as gene expression[1] and signal transduction[2]. In allosteric regulation, the association between a biological macromolecule (typically a protein[3,4] or RNA[5]) and its substrate is controlled by allosteric modulators, which act as activators[3] or inhibitors[6], resulting in either an up-regulated or down-regulated activity, respectively. Over the past two decades, allosteric regulation has garnered increasing interest across a broad research community, primarily due to its potential in developing allosteric drugs[7,8] and allosteric antibodies[9,10]. These offer promising therapeutic advantages for some of the most difficult-to-treat human neurological and psychiatric

disorders[11]. Due to the inherently limited programmability of protein dynamics, the ability to rationally design synthetic protein molecules with allosteric control capabilities remains constrained. In contrast, synthetic nucleic acid constructs, benefiting from their exceptional programmability[12-15], have emerged as ideal molecules for rational allosteric design[16-19]. By applying well-established design principles of synthetic nucleic acids and the extensive toolkits of DNA nanotechnology[20-24], engineered DNA constructs can be designed to recognize a variety of specific modulator—including biological, chemical, and even physical ones[25]—with high precision and functional control. Consequently, DNA-based allosteric systems represent a powerful strategy for various biomolecular detection tasks, offering levels of complexity and controllability that surpass those of their natural counterparts.

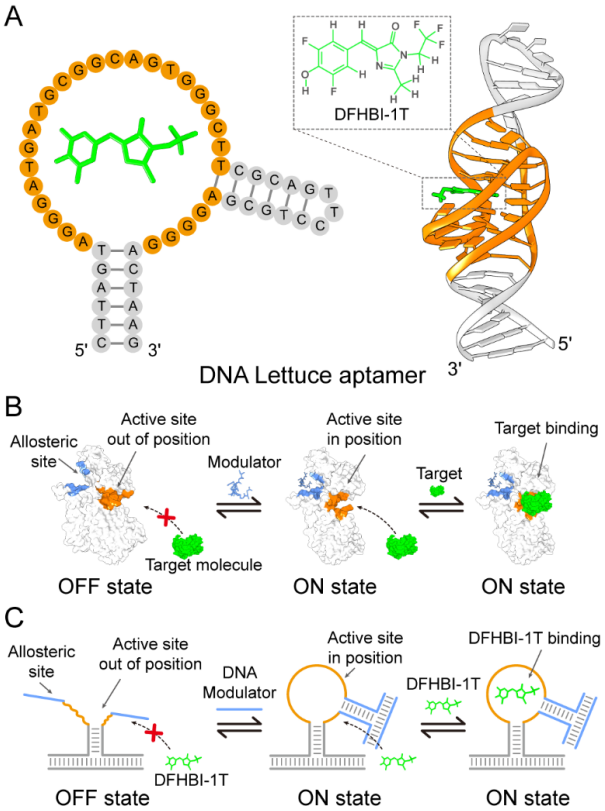

Fig. 1 Allosteric nano-switches based on fluorescent DNA aptamer—Lettuce. A, strand diagram and 3D structure (PDB ID: 8FHX) of DNA Lettuce aptamer, sequence in orange depicts the binding pocket of aptamer ligand—DFHBI-1T. **B**, Schematics of allosteric regulation. The conformation switching from the blocked state (OFF state) to the open state (ON state) is triggered upon allosteric modulator binding. **C**, DNA-based allosteric nano-switches regulated by DNA modulators.

In this study, we successfully designed a series of allosteric nano-switches (Fig. 1) based on the recently reported fluorescent DNA aptamer—Lettuce[26]. Lettuce functions as a GFP mimic, producing green fluorescence upon binding to its ligand, DFHBI-1T, under appropriate excitation conditions. The aptamer comprises a core DFHBI-1T binding pocket, whose formation primarily depends on the stability of two flanking stems. We designed and constructed split aptamers whose assembly is mediated by a stable constituent three-arm

junction[27], serving as the basic allosteric nano-switches. Prior to three-arm junction formation, the split aptamer adopts a loose conformation unable to form a complete binding pocket and bind to its ligand. Upon regulation by a target strand acting as an external allosteric modulator, the three-arm junction forms, leading to the reconstitution of the integral binding pocket and subsequent stable interaction with DFHBI-1T, thereby enabling fluorescence emission.

Through systematic screening of a set of synthetic DNA nano-switches, we specified a clear-cut fluorescent ON-OFF transition between well-defined conformational states. Subsequently, we enabled reversible regulation of fluorescent output by integrating toehold-mediated strand displacement into our design framework. By extending this strategy to incorporate multiple allosteric modulators, we successfully implemented a set of basic Boolean logic operations and their complex combinations. Finally, due to their excellent structure-dependent fluorescent properties, we integrated the allosteric DNA aptamers into light-up DNA nanostructures to facilitate characterization of nanostructure morphologies.

2. Results

2.1 Rational design and screening of allosteric fluorescent DNA nano-switches

We carefully specified ON and OFF allosteric states of fluorescent DNA nano-switch regulated by DNA modulators. As shown in Fig. 2A, the DNA Lettuce aptamer comprises three structural domains: two double-helical stems (P1 and P2, depicted in gray) and a ligand binding pocket (depicted in orange) positioned between P1 stem and P2 stem. With multiple guanines embedded in its sequence, the binding pocket forms a two-layer antiparallel G-quadruplex structure[26]. We hypothesize that stable formation of both P1 and P2 is essential for the proper conformation and function of the binding pocket. Specifically, stable P1 or P2 would reinforce the structural integrity of the binding pocket and enable fluorescence, whereas unstable P1 and P2 compromise fluorescence. To test the hypothesis, we designed nano-switches with extended P1 and P2 stems of varying lengths, regulated by a DNA modulator strand for allosteric control. A three-arm junction was incorporated into the nano-switch, where P1 (or P2) serves as one arm (Fig. 2B and D, Supplementary Figs. S1-S4), with its stability dependent on the formation of the other two arms. The formation of the other two arms is regulated by a modulator strand. Without modulator strand, the P1 stem remains unstable, maintaining the binding pocket of the nano-switch in OFF state. After allosteric transition triggered by the modulator strand, stable P1 stem formation switches the nano-switch to ON state and induces fluorescence.

We first designed two extended tails (15-bp) on P1 stem. These tails formed two arms upon collectively binding a 30-nt modulator strand, thereby forming a full three-arm junction with P1. With P2 fixed at 10 bp, we screened P1 variants of gradient lengths (0 to 10-bp) to evaluate the ON-OFF transition between allosteric states regulated by the same modulator strand. Systematic screening and quantitative analysis of fluorescence intensity measurements enabled the identification of optimal variants (Fig. 2C, Supplementary Table. S1).

While no transition was observed for seven negative variants, four positive variants (x=1, 2, 3, 4) exhibited successful ON-OFF fluorescence transition upon modulator binding. Initially,

these four variants showed very weak fluorescence (normalized intensity below 0.5) without modulator. However, strong fluorescence (normalized intensity above 0.5) was detected upon modulator binding, marking a clear allosteric transition. In contrast, variants with P1 length ≥ 5 nt (x=5, 6, 7, 8, 9, 10) displayed a permanent ON state due to a stable P1 stem even without modulator binding (no three-arm junction). This ambiguous ON-OFF state rendered allosteric regulation unattainable. Finally, variants lacking P1 stem (x=0) maintained weak fluorescence intensity regardless of the presence of modulators, also preventing allosteric regulation. This absence of regulation might be attributed to disruption of the binding pocket conformation by the arm junction.

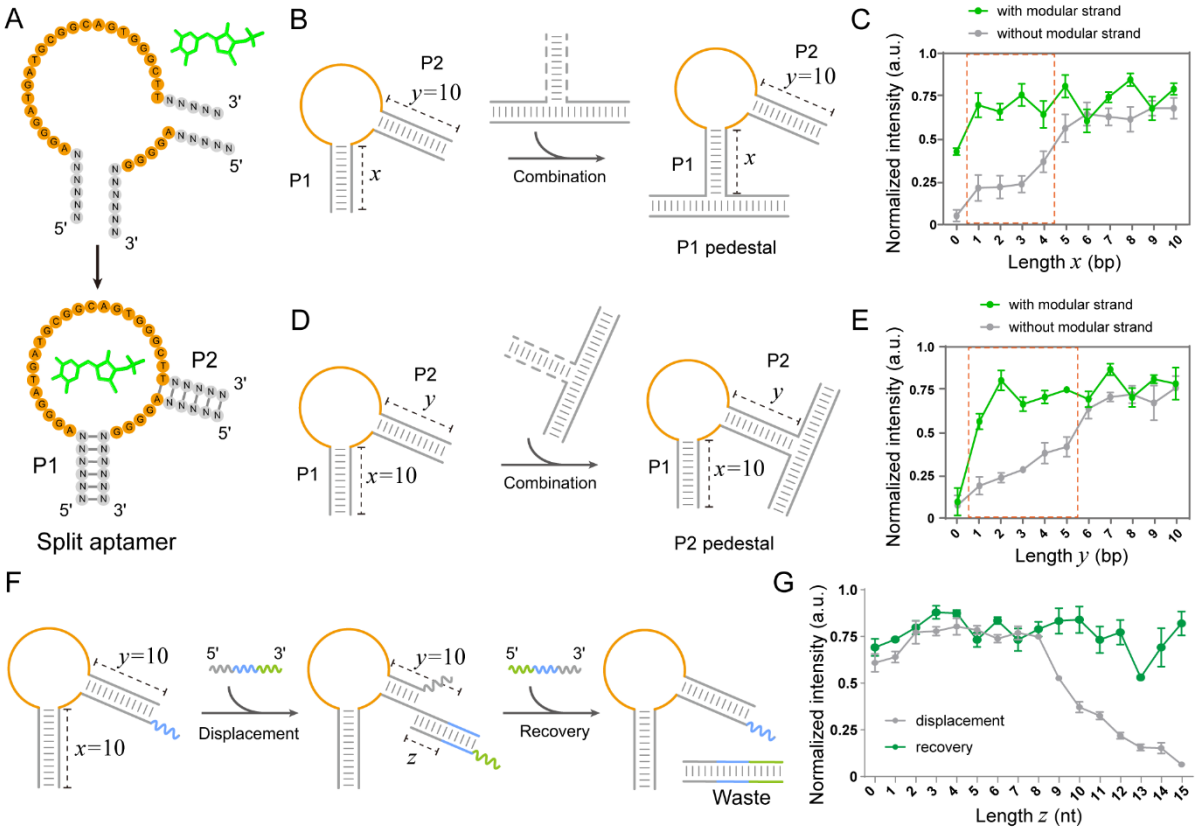

Fig. 2 Design and screening of DNA allosteric aptamers. A, Strand diagram of a split DNA Lettuce aptamer. Sequence in orange depicts the binding pocket of aptamer ligand—DFHBI-1T. **B-C**. Design schematics (**B**) and screening results (**C**) of the allosteric nano-switch regulated by P1 formation. **D-E**. Design schematics (**D**) and screening results (**E**) of the allosteric nano-switch regulated by P2 formation. **F-G**. Design schematics (**F**) and screening results (**G**) of the reverse allosteric regulation.

With a similar rationale, we screened a set of P2 variants with gradient lengths (0 to 10-bp) to evaluate the modulator-regulated ON-OFF transition between allosteric states (Fig. 2E, Supplementary Table. S2). Five positive variants (x=1, 2, 3, 4, 5) were identified, showing successful fluorescence transition upon modulator binding. For these variants, only weak fluorescence (normalized intensity below 0.5) was detected without modulator, while strong fluorescence (normalized intensity above 0.5) was detected upon modulator binding, resulting in a prominent transition. Variants with P2 lengths ≥ 6 nt (y=6, 7, 8, 9, 10) displayed failed allosteric regulation, remaining in a permanent ON state due to sufficient P2 stem stability

without modulator binding (no three-arm junction), resulting in strong fluorescence intensity independent of modulators. The variants without a P2 stem (y=0) showed ambiguous ON-OFF states, exhibiting weak fluorescence intensity even with modulators present. In conclusion, a clear ON-OFF transition was successfully achieved by designing and screening variants with pre-set P1 or P2 stems of different lengths. Given the comparable performance of P1-directed and P2-directed regulation, we selected P2-directed regulation for subsequent experiments.

To demonstrate the programmability of these allosteric DNA aptamer, we then incorporated toehold-mediated strand displacement into the design scheme to achieve a reversible allosteric regulation. Specifically, we designed an allosteric nano-switch where the P1 stem formed a stable 10-bp duplex, and the P2 stem formed a stable 10-bp duplex with an additional toehold region (Fig. 2F). This nano-switch features stable P1 and P2 stems with a well-defined binding pocket capable of ligand binding and strong fluorescence emission. Upon introducing a displacement strand that binds to the toehold and initiates strand displacement, the P2 stem dissociates and disrupts the binding pocket, resulting in decreased fluorescence activity. Subsequent addition of an anti-displacement strand fully complementary to the displacement strand, restores the P2 stem as a stable duplex. This generates a functional binding pocket and consequently recovers fluorescence activity (Fig. 2G, Supplementary Table. S3).

2.2 Boolean logic operations based on allosteric DNA aptamer

With the successful implementation of toehold-mediated strand displacement in allosteric operations, our next goal was to use an allosteric DNA aptamer to achieve Boolean logic operations and complex nanocircuits, with the seamless incorporation of existing DNA nanotechnology design frameworks. Leveraging strand complementation and displacement, we implemented six basic logic gates (AND, OR, XOR, NAND, NOR and XNOR gates, Fig. 3). These logic gates fall into two categories: the first category (AND, OR, XOR) has an initial OFF state (output=0) when no inputs are present (input = [0, 0]). The second category (NAND, NOR, XNOR) has an initial ON state (output=1) when no inputs are present (input = [0, 0]).

The first category gates were constructed using an allosteric DNA aptamer design with stable P2 stems before adding modulator strands as inputs. When modulator strands were added, a conformational change stabilized the P2 stem, generating a TRUE value (output = 1). Conversely, the second category gates used an aptamer design with initially stable P2 stems. These stems became destabilized when one or both strands within the P2 stem were displaced by specific input strands. Upon addition of these displacement strands, the resulting deformation of the P2 stem and binding pocket led to fluorescence loss, generating a FALSE value (output = 0).

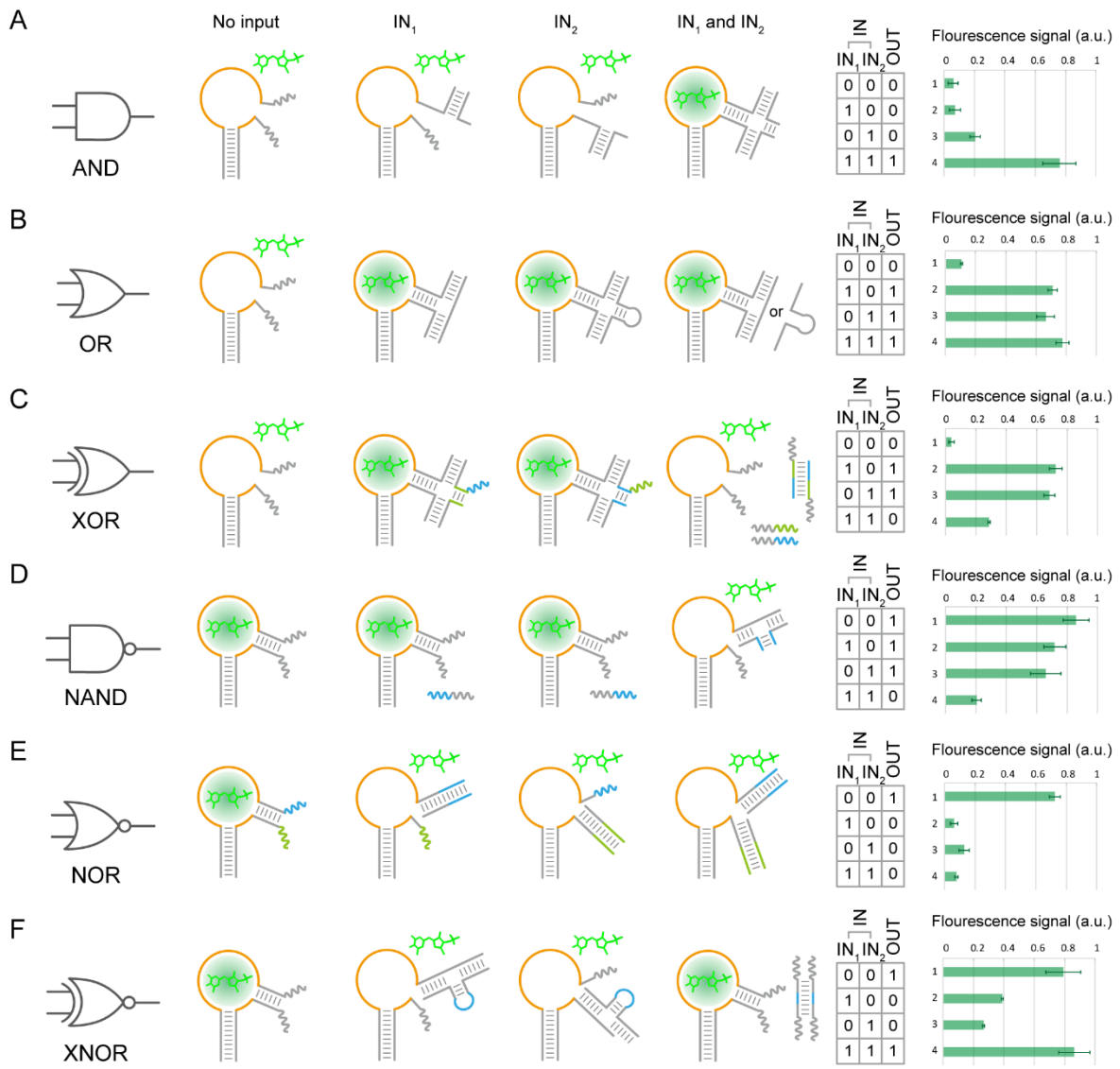

Fig. 3 Six types of Boolean logic operations with allosteric nano-switches. A, AND gate. **B**, OR gate. **C**, XOR gate. **D**, NAND gate. **E**, NOR gate. **F**, XNOR gate. The logic gate was displayed in OFF or ON state without inputs, with IN_1, IN_2 or both inputs. Left: design principle; right: truth table and fluorescence analysis.

Taking the AND logic gate design as an example (Fig. 3A), an unstable P2 stem was configured as a 2-bp duplex segment flanked by two 15-nt unpaired single-stranded toeholds. In the absence of inputs (input = [0, 0]), the instability of P2 resulted in a deformed binding pocket, leaving the DNA aptamer in an OFF state with no fluorescent activity (output = 0). Two input strands were designed such that each bind to one toehold of the P2 stem, with the inputs themselves connected via a duplex binding region. When either input was present alone (input = [1, 0], [0, 1]), the P2 stem remained unstable, yielding no fluorescence (output = 0). Only when both inputs were available (input = [1, 1]) did a four-way junction form, stabilizing the P2 stem and creating a functional binding pocket. This switched the DNA aptamer to an ON state (output = 1). Outputs were recorded via fluorescence measurements and statistically analyzed. Similarly, OR, XOR, NAND, NOR, and XNOR gates were implemented by reconfiguring the nano-switch and strand displacement pathways (Fig. 3B-F, Supplementary Table. S4).

2.3 Combinatorial nanocircuits based on allosteric DNA aptamer

Building on the successful implementation of basic Boolean operations, we next aimed to construct a more complex allosteric circuit implementing a three-input combinatorial BUFFER function. We first tested the orthogonality of the allosteric regulation using 10 different pairs of nano-switches (Apt-1 ~ Apt-10) with their corresponding modular strands (M-1 ~ M-10). The ten modular strands had distinct sequences, ensuring each nano-switch could only be modulated by its specific modular strand (i.e., Apt-1 is modulated by M-1, Apt-2 is modulated by M-2). We measured the fluorescence intensity of each nano-switch in the presence of all ten modular strands and found no significant crosstalk (Fig. 4A, Supplementary Table. S5), demonstrating the orthogonality of this allosteric regulation strategy. We then designed a combinatorial BUFFER function with three inputs, as illustrated in Fig. 4B-D. In this circuit, each of the three BUFFER gates is controlled only by its target input and not by the other two inputs (IN1 for the 1st BUFFER gate; IN2 for the 2nd BUFFER gate; IN3 for the 3rd BUFFER gate). This combinatorial BUFFER function exhibited increasing fluorescence intensity levels with an increasing numbers of active inputs (Fig. 4E).

We then constructed another complex allosteric circuit implementing the three-input MAJORITY function—a combinational circuit that generates TRUE value (or 1) when the majority of inputs (≥ 2) are added, otherwise the outputs are FALSE (or 0). To implement this, we integrated three orthogonal AND gates and one OR gate. Each AND gate was constructed using a co-allosteric regulation mechanism in which both the P1 and P2 stems of a nano-switch are controlled by two different modular strands. Each AND logic gate (representing one nano-switch) is regulated by two inputs, with every pair of gates sharing one common input, as illustrated in Fig. 4F-I. Specifically: IN_A and IN_B regulate the first AND gate; IN_B and IN_C regulate the second AND gate; IN_C and IN_A regulate the third AND gate. As expected, no fluorescence was detected in the absence of any inputs. When a majority of inputs (2 or 3 inputs) were present, most nano-switches underwent conformational changes, producing green fluorescence. Conversely, the system maintained its original conformation with any single input, and no fluorescence was detected (Fig. 4F-J, Supplementary Table. S6).

With an immense sequence space defined by a four-letter code (4^N, where N is the length of modulator strand), we envision that many more distinct species of nano-switches could be created to implement advanced algorithms and molecular computing tasks.

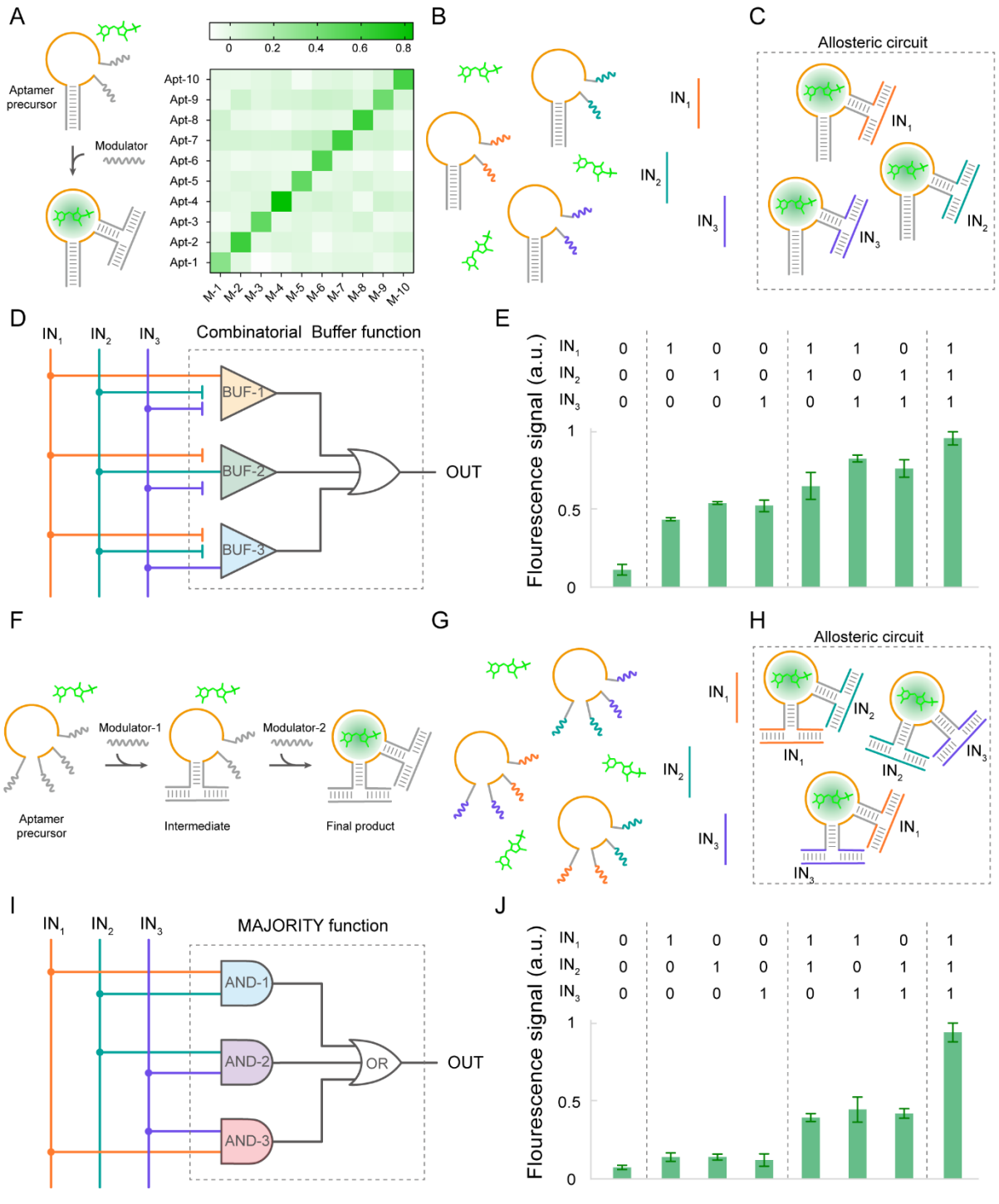

Fig. 4 Programmable nanocircuits with allosteric nano-switches. A, Orthogonality test of ten different allosteric DNA aptamers with their corresponding modulator strands. **B-C**, Schematics of the combinatorial BUFFER nanocircuits, involving (**B**) three different allosteric aptamers and three different modular strands as inputs, and (**C**) allosteric circuit system (Aptamer-1 coupled with IN_1; Aptamer-2 with IN_2; Aptamer-3 with IN_3). **D**, Schematics of the combinatorial BUFFER function. **E**, Statistical analysis of the allosteric nanocircuits in response to different combinations of inputs. The dash lines are set to distinguish four levels of inputs: no input, single input, double inputs and triple inputs. **F**, Schematics of the aptamers coregulated by two allosteric modulators. **G-H**, Schematics of the MAJORITY nanocircuits, involving (**G**) three different allosteric aptamers and three different modular strands as inputs, and (**H**) allosteric circuit system (Aptamer-1 coupled with IN_1 and

IN_2; Aptamer-2 with IN_2 and IN_3; Aptamer-3 with IN_3 and IN_1). **I**, Schematics of the combinatorial MAJORITY function. **J**, Statistical analysis of the allosteric nanocircuits in response to different combinations of inputs. The dash lines are set to distinguish four levels of inputs: no input, single input, double inputs and triple inputs.

2.4 Light-up DNA nanostructures with allosteric DNA aptamer

The programmable and controllable fluorescence properties prompt us to apply our allosteric aptamers as a reporter system for the fluorescent imaging of DNA nanostructures. Conventional fluorescent imaging of DNA nanostructures relies on chemically modified fluorophore-conjugated probes, where fluorescence intensity depends solely on fluorophore properties and is therefore non-adjustable. For example, the collective intensity of a nanostructure target associated with a probe or probe complex is independent of the probe configurations and clustering status. In contrast, our allosteric aptamer produces fluorescent ON/OFF signals in direct response to configurational transition, with the structural properties of DNA nanostructures serving as the foundation for its fluorescent functionality.

To validate this approach, we used a 10-helix bundle (10-HB) DNA origami as a representative DNA nanostructure and evaluated its fluorescent performance when modified with allosteric DNA aptamers. We incorporated allosteric DNA aptamers into 16 pairs of staples along a constituent helix (Helix-9) of the 10-HB origami (Supplementary Fig. S5), creating a modified design—10-HB-apt. In a well-folded state where all staples bind to scaffolds as designed, the allosteric aptamer adopts a proper binding pocket configuration, enabling the nanostructure to exhibit high fluorescent intensity. When the morphological state of nanostructure is compromised (e.g., due to degradation or denaturation), misfolded staples disrupt the aptamer binding pocket, resulting in fluorescence loss. For comparison, we appended the same 16 modification sites with FAM-labeled DNA probes in a 10-HB-pro design as a control group. To test whether the structural integrity of 10-HB affects fluorescence, we measured the fluorescent intensity of both designs after treatment with DNase I-induced degradation and heat-induced denaturation, respectively (Supplementary Figs. S8-S9).

DNase I is an endonuclease that degrades both single- and double-stranded DNA into dinucleotide, trinucleotide, and oligonucleotide products[28,29], which can significantly compromise the structural integrity of DNA nanostructures[30,31]. Agarose gel electrophoresis revealed dissociated structures after degradation with DNase I (at a final concentration of 20 Unit/mL). Consistently, fluorescence measurement showed signal loss in 10-HB-apt after DNase I treatment, while the signal remained constant for the 10-HB-pro control despite structural decay. Similarly, heating (40-80°C) produced analogous structure-dependent effects. The fluorescence signal of 10-HB-apt was significantly more sensitive to denaturation by heating than that of 10-HB-pro (Supplementary Table. S7). These degradation and denaturation tests demonstrated that the fluorescent functionality of allosteric DNA nanostructures depends on proper structure configuration.

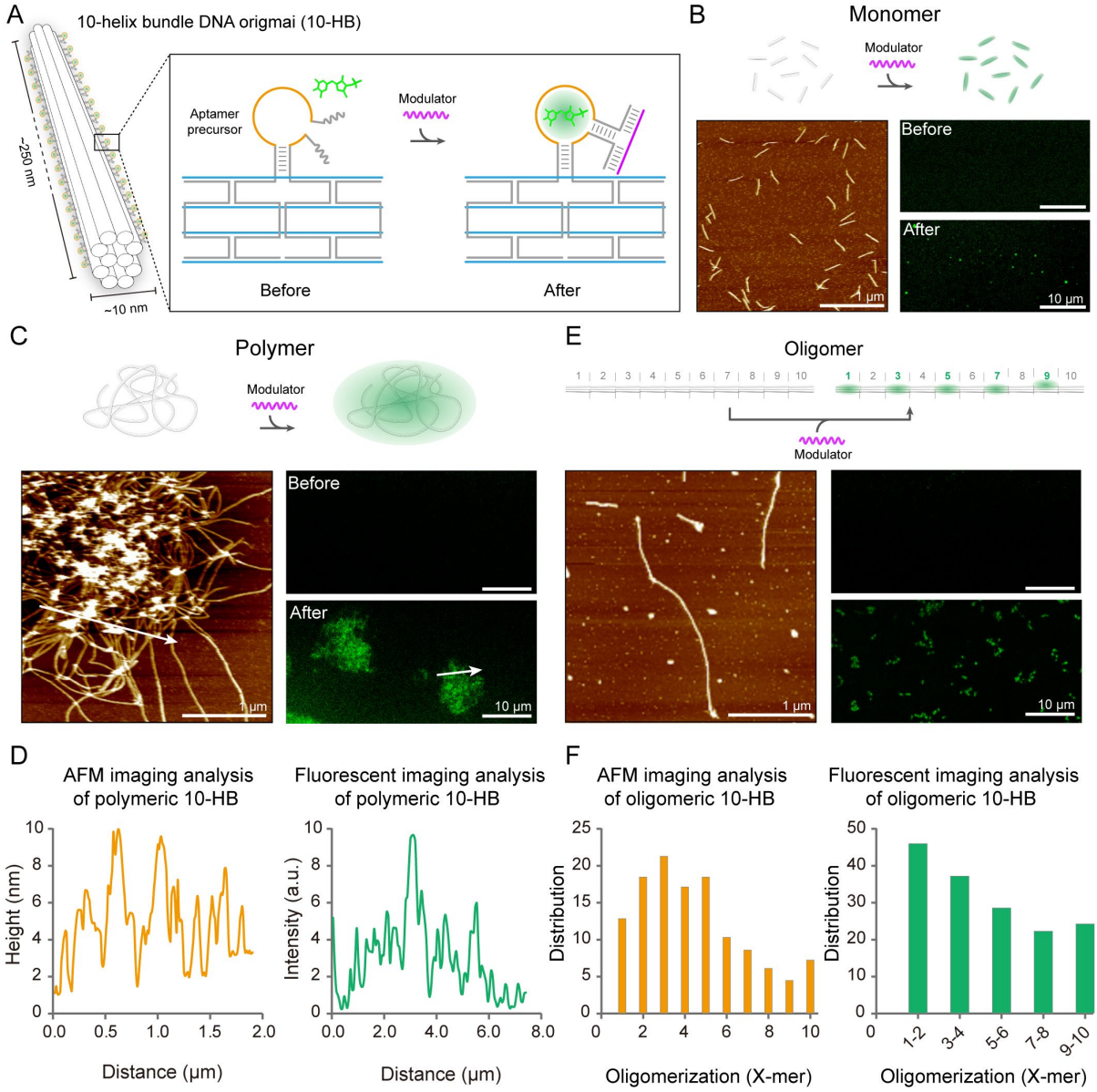

Fig. 5 Light-up nanostructures with allosteric DNA aptamer. A, Schematics of the 10-HB origami appended with allosteric aptamers at 32 sites along two helices. **B, C, E**, Schematics (top) depicting the inducible lighting-up of monomeric (**B**), polymeric (**C**) and oligomeric (**E**) 10-HB origami. Bottom-left: AFM imaging results; Bottom-right: CLSM imaging results. Scale bars for AFM images: 1 μm; scale bars for CLSM images: 10 μm. **D, F**, AFM imaging analysis (left) and fluorescent imaging analysis of polymeric (**D**) and oligomeric (**F**) 10-HB origami. For statistical analysis in (**F**), N is ~200.

Next, we implemented our allosteric strategy to achieve inducible lighting-up of DNA nanostructures. To achieve higher fluorescence intensity under fluorescence microscopy, we incorporated allosteric DNA aptamers into 32 pairs of staples within two constituent helices of the 10-HB origami (16 pairs along Helix-9 and 16 pairs along Helix-0, Fig. 5A and Supplementary Fig. S5). All 32 sites contain the same aptamer regulatory sequence, which binds to identical modulator oligos. In the absence of the modulator, the allosteric aptamer lacks a stable binding pocket and emits no fluorescence. After introducing the modulator into the system, its binding to the two tails of the P2 stem induced the aptamer binding pocket into an

ON state, triggering fluorescence emission from the nanostructures.

The 10-HB origami was engineered to adopt three distinct clustering states—monomer, polymer, and oligomer—by programming intermolecular edge-edge interactions using complementary sticky ends between neighboring origami units (Supplementary Figs. S6-S7). Monomeric 10-HB origami displayed dispersed rod-like structures under atomic force microscopy imaging (AFM) and consistently appeared as dispersed bright dots (due to the diffraction limit, the ~250 nm 10-HB origami can only present a round spots under optical microscopy) under confocal fluorescence microscopy (CLSM) after allosteric regulation by modulators (Fig. 5B, Supplementary Figs. S10-S11). Polymeric 10-HB origami formed micrometer-scale clusters observable under both AFM and CLSM (Fig. 5C, Supplementary Figs. S12-S13), with similar density distributions (height distribution under AFM and intensity distribution under CLSM). For the oligomeric design, ten variants of the 10-HB origami monomers (O1~O10, Supplementary Fig. S7) were designed. These origami shared the same structural core but featured ten distinct groups of connection edge staples, enabling specific end-to-end assembly into long linear structures. To generate a fluorescent dotted-line pattern, we modified O1/O3/O5/O7/O9 with allosteric aptamer while leaving O2/O4/O6/O8/O10 unmodified. During a one-pot assembly of these 10-HB variants, we observed a distribution of oligomer lengths (Fig. 5E, Supplementary Figs. S14-S15), indicating varying degrees of oligomerization. The consistent structural distributions revealed by both AFM and CLSM validate the feasibility of using allosteric aptamer to characterize DNA nanostructures.

After the successfully demonstration of inducible lighting-up of DNA nanostructures using allosteric aptamers, we next implemented this strategy to detect target mRNAs. For detection, 16 pairs of staples along Helix-9 of the 10-HB origami (Fig. 6A) were modified with allosteric aptamers targeting 16 distinct binding sequences. These aptamers on a single 10-HB origami were designed to recognize and bind in tandem to 16 target sites (20 nt per site) on a specific mRNA molecule, enabling 1:1 target recognition. We tested the performance of this allosteric aptamer-functionalized DNA origami using three in vitro transcribed mRNA targets (designated mRNA-1, mRNA-2, and mRNA-3). The functionalized 10-HB origami initially presented no obvious fluorescence signal in the absence of target mRNA and generated a positive signal upon target binding, though the fluorescent intensity remained limited (Fig. 6B, Supplementary Fig. S16A-B). We hypothesized that this limited intensity resulted from intrinsic mRNA secondary structures compromising the accessibility of target mRNA sites for allosteric aptamers. To address this, we treated mRNA targets with a denaturing condition (heating at 80°C followed by rapid cooling on ice) to disrupt secondary structures and minimize refolding before hybridization with the allosteric aptamers. Consequently, denatured mRNA-1 and mRNA-2 targets exhibited significant fluorescence enhancement (Fig. 5C). Moreover, mRNA-1 induced higher intensity than mRNA-2 did, likely due to its weaker secondary structure.

However, the binding of denatured mRNA-3 did not yield a significant enhancement in fluorescence intensity, despite its likely minimal secondary structure (Supplementary Fig. S16C). Given that mRNA-3 is only ~500-nt long, a tightly stretched configuration with 10-nt linkers between binding segments is necessary for it to fully bind all 16 aptamers on the 10-HB origami. Consequently, skipping certain binding segments was deemed inevitable, resulting in

reduced fluorescent intensity for mRNA-3. Increasing the concentration ratio of mRNA to 10-HB origami counteracted the effect of omitted aptamer binding, leading to a compensatory increase in fluorescence intensity (Supplementary Fig. S16D and Table. S8). Therefore, designing an appropriate aptamer density to match a specific mRNA length is preferable.

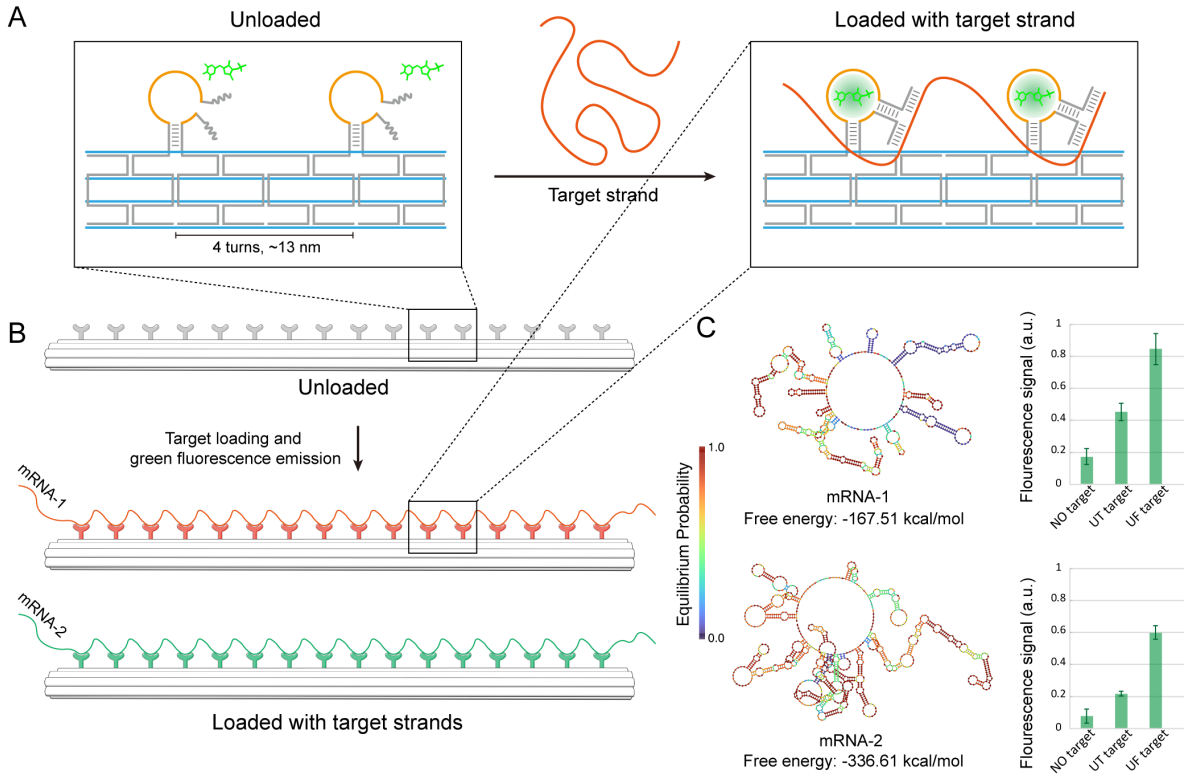

Fig. 6 mRNA detection with lighting-up DNA nanostructures. A-B, Schematics of the 10-HB origami appended with allosteric aptamers at 16 sites along one helix that can recognize and bind to target mRNA. **C**, Left, schematics of the secondary and energy landscape of mRNA-1 and mRNA-2. Right, statistical analysis of fluorescence intensity of 10-HB origami before and after binding to target mRNA. UT target, untreated mRNA target; UF, unfolded mRNA targets after heating and crash-cooling on ice. Errors bars, S.E.M..

3. Conclusion

Building on programmable allosteric regulation, we created a series of synthetic nucleic acid nano-switches with precisely controlled fluorescence ON-OFF transition. By employing a single-stranded DNA modulator targeting the allosteric site, we enabled adjustable fluorescent readouts in these custom-designed DNA nano-switches. This robust system allows for diverse allosteric regulatory functions, including designated allosteric transitions, reverse allosteric regulation, and complex logic operations.

The study here offers a highly adaptable design framework for nucleic acid nanotechnology, highlighting its extensibility and vast application potential. By modular integration of diverse functional DNA sequences responsive to environmental cues (expanded allosteric modulators, including proteins, ions, pH, light, etc.), the core allosteric switching mechanism could become

a universal platform. Such a universal platform can allow researchers to "plug in" specific sensors tailored to desired biological, chemical and physical signals, transforming allosteric aptamers into versatile fluorescent detectors or actuators, pointing directly toward sophisticated applications in bioimaging and diagnostics. Beyond the fluorescence-based readouts demonstrated in this study, the framework is readily adaptable for allosterically regulating a wide range of biochemical activities by substituting the fluorescent aptamer core with other functional DNAs or RNAs. This flexibility opens new avenues for engineering modular riboswitches, ribozymes, and RNA logic circuits with customized responses.

By synthetically building these allosteric devices from scratch, the platform also offers an approach for researchers to investigate how structure dictates function and dynamics in nucleic acids and other biomolecular systems. This synthetic biology approach provides a simplified system to dissect allostery principles that might be obscured in more complex natural systems. Attempting to rationally engineer or re-engineer natural biomolecules (proteins, RNAs) or complexes using similar principles can lead to deeper mechanistic understanding of their function and uncover previously unrealized application potential in both biology (e.g., designing novel enzymes, metabolic pathways) and material science (e.g., creating programmable biomaterials, self-assembling nanostructures).

In sum, the study here offers an extensible synthetic framework that enables the creation of sophisticated DNA devices for potential applications, while simultaneously providing fundamental insights and design principles. These principles, in turn, empower the rational engineering of both synthetic and naturally occurring systems, advancing both basic scientific understanding and technological innovation across disciplines.

Acknowledgements

This work is supported by: National Key R&D Program of China (grant No. 2021YFF1200200), National Natural Science Foundation of China (grant No. 31770926,), Tsinghua University Spring Breeze Fund, and Tsinghua University-Peking University Joint Center for Life Sciences (to B.W.); National Key R&D Program of China (grant No. 2023YFC2306300), National Natural Science Foundation of China (grant No. 32225019, 92357304, 32394003), Beijing Natural Science Foundation (grant No. 5222010), Tsinghua -Peking Joint Center for Life Sciences, the Institute for Immunology, and School of Basic Medical Sciences at Tsinghua University (to W.Z.); National Key R&D Program of China (grant No. 2021YFA0909400), National Natural Science Foundation of China (grant No. 22225402, 32341017), Leading Innovative and Entrepreneur Team Introduction Program of Zhejiang Province (grant No. 2024R01005), Hangzhou Institute of Medicine, Chinese Academy of Sciences (to D.H.); Research Grant Council of Hong Kong (grant No. 14207421), Department of Biomedical Engineering, Chinese University of Hong Kong (to Z.G.).

Conflict of Interest

The authors declare no conflict of interest.

Data availability

All the data presented in the article and Supplementary Information are available from the corresponding authors upon reasonable request.

Author contributions

T.Z. and X.Q. conceived the study and conducted the experiments. J.Z. and H.C. assisted with the experiment design. T.B. and W.W. designed the 10HB origami. Y.W. assisted with sample preparation. T.Z., B.W., W.Z., D.H., Z.G. supervised the project. All authors analyzed the data and wrote the manuscript.

References

1 Weikum, E. R., Knuesel, M. T., Ortlund, E. A. & Yamamoto, K. R. Glucocorticoid receptor control of transcription: precision and plasticity via allostery. *Nat Rev Mol Cell Biol* **18**, 159-174 (2017).

2 De Smet, F., Christopoulos, A. & Carmeliet, P. Allosteric targeting of receptor tyrosine kinases. *Nat Biotechnol* **32**, 1113-1120 (2014).

3 Ahmed, M. H., Ghatge, M. S. & Safo, M. K. Hemoglobin: Structure, Function and Allostery. *Subcell Biochem* **94**, 345-382 (2020).

4 Shen, S. et al. Allosteric modulation of G protein-coupled receptor signaling. *Front Endocrinol (Lausanne)* **14**, 1137604 (2023).

5 Ooms, M., Huthoff, H., Russell, R., Liang, C. & Berkhout, B. A riboswitch regulates RNA dimerization and packaging in human immunodeficiency virus type 1 virions. *J Virol* **78**, 10814-10819 (2004).

6 Kemp, R. G. & Foe, L. G. Allosteric regulatory properties of muscle phosphofructokinase. *Mol Cell Biochem* **57**, 147-154 (1983).

7 Guarnera, E. & Berezovsky, I. N. Allosteric drugs and mutations: chances, challenges, and necessity. *Curr Opin Struct Biol* **62**, 149-157 (2020).

8 Abdel-Magid, A. F. Allosteric modulators: an emerging concept in drug discovery. *ACS Med Chem Lett* **6**, 104-107 (2015).

9 Fournier, L., Guarnera, E., Kolmar, H. & Becker, S. Allosteric antibodies: a novel paradigm in drug discovery. *Trends Pharmacol Sci* **46**, 311-323 (2025).

10 Fournier, L. et al. Discovery of potent allosteric antibodies inhibiting EGFR. *MAbs* **16**, 2406548 (2024).

11 Conn, P. J., Lindsley, C. W., Meiler, J. & Niswender, C. M. Opportunities and challenges in the discovery of allosteric modulators of GPCRs for treating CNS disorders. *Nature Reviews Drug Discovery* **13**, 692-708 (2014).

12 Seeman, N. C. & Sleiman, H. F. DNA nanotechnology. *Nature Reviews Materials* **3** (2017).

13 Seeman, N. C. Nucleic acid junctions and lattices. *J Theor Biol* **99**, 237-247 (1982).

14 Rothemund, P. W. Folding DNA to create nanoscale shapes and patterns. *Nature* **440**, 297-302 (2006).

15 Lin, C., Liu, Y., Rinker, S. & Yan, H. DNA tile based self-assembly: building complex nanoarchitectures. *Chemphyschem* **7**, 1641-1647 (2006).

16 Zhang, T. & Wei, B. Rational Design of Allosteric Nanodevices Based on DNA Triple Helix. *J Am*

Chem Soc **143**, 16693-16699 (2021).
17 Ricci, F., Vallee-Belisle, A., Porchetta, A. & Plaxco, K. W. Rational design of allosteric inhibitors and activators using the population-shift model: in vitro validation and application to an artificial biosensor. *J Am Chem Soc* **134**, 15177-15180 (2012).
18 Tang, J. & Breaker, R. R. Rational design of allosteric ribozymes. *Chem Biol* **4**, 453-459 (1997).
19 Wang, C., Yue, L. & Willner, I. Controlling biocatalytic cascades with enzyme–DNA dynamic networks. *Nature Catalysis* **3**, 941-950 (2020).
20 Zhang, D. Y., Hariadi, R. F., Choi, H. M. & Winfree, E. Integrating DNA strand-displacement circuitry with DNA tile self-assembly. *Nat Commun* **4**, 1965 (2013).
21 Padilla, J. E. et al. A Signal-Passing DNA-Strand-Exchange Mechanism for Active Self-Assembly of DNA Nanostructures. *Angew Chem Int Ed Engl* **54**, 5939-5942 (2015).
22 Garg, S., Chandran, H., Gopalkrishnan, N., LaBean, T. H. & Reif, J. Directed enzymatic activation of 1-D DNA tiles. *ACS Nano* **9**, 1072-1079 (2015).
23 Zhang, D. Y. & Seelig, G. Dynamic DNA nanotechnology using strand-displacement reactions. *Nat Chem* **3**, 103-113 (2011).
24 Zhang, H. et al. Programming chain-growth copolymerization of DNA hairpin tiles for in-vitro hierarchical supramolecular organization. *Nat Commun* **10**, 1006 (2019).
25 Wang, F., Willner, B. & Willner, I. DNA-based machines. *Top Curr Chem* **354**, 279-338 (2014).
26 Passalacqua, L. F. M. et al. Intricate 3D architecture of a DNA mimic of GFP. *Nature* **618**, 1078-1084 (2023).
27 Woods, K. C., Martin, S. S., Chu, V. C. & Baldwin, E. P. Quasi-equivalence in site-specific recombinase structure and function: crystal structure and activity of trimeric Cre recombinase bound to a three-way Lox DNA junction. *J Mol Biol* **313**, 49-69 (2001).
28 Kunitz, M. Crystalline desoxyribonuclease; isolation and general properties; spectrophotometric method for the measurement of desoxyribonuclease activity. *J Gen Physiol* **33**, 349-362 (1950).
29 Vanecko, S. & Laskowski, M., Sr. Studies of the specificity of deoxyribonuclease I. III. Hydrolysis of chains carrying a monoesterified phosphate on carbon 5'. *J Biol Chem* **236**, 3312-3316 (1961).
30 Xu, Y., Yan, Z. S., Ma, Y. Q. & Ding, H. M. Topology- and size-dependent binding of DNA nanostructures to the DNase I. *Int J Biol Macromol* **257**, 128703 (2024).
31 Ramakrishnan, S. et al. Real-Time Observation of Superstructure-Dependent DNA Origami Digestion by DNase I Using High-Speed Atomic Force Microscopy. *Chembiochem* **20**, 2818-2823 (2019).